IEEE Access
Multidisciplinary | Rapid Review | Open Access Journal

Received July 18, 2019, accepted July 29, 2019, date of publication August 5, 2019, date of current version August 15, 2019.

Digital Object Identifier 10.1109/ACCESS.2019.2933016

Stability Research of Distributed Drive Electric Vehicle by Adaptive Direct Yaw Moment Control

HOUZHONG ZHANG[1], JIASHENG LIANG[1], HAOBIN JIANG[1,2], YINGFENG CAI[1], AND XING XU[1]

[1]Automotive Engineering Research Institute, Jiangsu University, Zhenjiang 212013, China
[2]School of Automobile and Traffic Engineering, Jiangsu University, Zhenjiang 212013, China

Corresponding author: Jiasheng Liang (2211804024@stmail.ujs.edu.cn)

This work was supported in part by the Six Talent Peaks Project of Jiangsu Province under Grant JXQC-042, in part by the Primary Research and Development Plan of Jiangsu Province under Grant BE2017129, in part by the National Key Research and Development Plan Program under Grant 2018YFB0104803, and in part by the Initial Funding for Advanced Talents at Jiangsu University under Grant 13JDG034.

ABSTRACT As one of the active safety technologies, stability control of vehicles has recently received great attention. In order to improve the handling stability of distributed drive electric vehicles under various extreme conditions, a direct yaw moment control (DYC) method based on a novel fuzzy sliding mode control (FSMC) is proposed. First, a linear 2DOF reference vehicle model as ideal value reference, a 7DOF vehicle model used for sideslip angle estimation, an electric-driving wheel model used to provide tire motion parameters based on CarSim platform are established. Then, FSMC is designed as the core decision-making layer of the control method to calculate the required additional yaw moment on the premise of estimating the sideslip angle. Four hub motors are allocated by the distribution method based on axle load proportion. Finally, under two typical working conditions, the four hub motors are allocated. Compared with traditional sliding mode control (SMC), the results show that FSMC can not only maintain vehicle stability more effectively under different working conditions, but also greatly reduce the occurrence of buffeting phenomenon, which has practical significance for engineering applications.

INDEX TERMS Direct yaw moment control, fuzzy sliding mode control, lateral stability, active safety control strategy, distributed drive electric vehicle.

I. INTRODUCTION

With advancements in society, automobile safety issues have been gradually emphasized, and the traditional safety concept is too passive to satisfy the current needs. Therefore, the concept of active safety is gradually being developed by various research institutions and enterprises [1]. As a kind of active safety control technology, a substantial amount of facts have proven that direct yaw moment control (DYC) has a remarkable control effect regarding the vehicle handling stability under extreme conditions, such as rapid steering wheel input, or at high speeds [2]. The calculation of the yaw moment is quite important in a DYC system. The value of an additional yaw moment fundamentally determines the control effect. Currently, the main calculation methods at the decision-making level are fuzzy control, fuzzy PID control and sliding mode control. As the design of fuzzy logic does not depend on the model of the controlled object at all, fuzzy control is applied to the nonlinear system in the research of Ding *et al.* and Li *et al.*, which obtain an ideal control effect [3], [4]. However, this method is too reliant on expert experience, and the direct fuzzy processing of information will cause a reduction in control accuracy and a decline in dynamic quality. In the research of Wang *et al.* and Jin *et al.*, the PID parameters are tuned using fuzzy control to adapt to different working conditions and achieve excellent robustness [5], [6]. However, a higher set of fuzzy rules and membership functions is required, and sometimes the control accuracy is even worse than that of PID control. SMC is used to calculate the additional yaw moment in the research of Wang *et al.*, Xiong *et al.* and Zhang *et al.* [7]–[9]. The difference between sliding mode control and other control methods is that the structure of the system is not fixed and can purposefully and dynamically change according to the current state of the system in the dynamic process, which forces the control system to move according to the state

The associate editor coordinating the review of this manuscript and approving it for publication was Rathinasamy Sakthivel.

trajectory of the predetermined sliding mode. This type of control has the advantage of fast response and does not need online identification of the system [10]. However, due to the problems of estimation and linear idealization in the process of mathematical modeling, a large switching gain is required to avoid the uncertainties caused by these problems, which will inevitably cause chattering. The chattering phenomenon causes the state of the actuator to continuously change. Therefore, this chattering will cause great damage to electronic and mechanical components and substantially reduces the service life in the long term. Once the switching gain coefficient is determined, it cannot be changed, which will substantially limit the control effect of SMC on vehicles under different conditions. A few scholars have studied the two previously mentioned problems. Tota *et al.* have employed integral sliding mode control (ISMC). In this unique ISMC case, the equivalent control is generated, which guarantees chattering alleviation and enhances the controller tracking performance in transient conditions [11]. Lu *et al.* proposed the second-order for the singular terminal sliding mode load observer to achieve the purpose of anti-disturbance speed control and to further improve the robustness of the control system [12].

This paper aims to comprehensively study a new method. Based on the previous analysis, if the advantages of both fuzzy logic algorithms and SMC are combined, an adaptive fuzzy sliding mode control (FSMC) method is designed. FSMC can be applied to the DYC of an automobile, which can substantially reduce the chattering caused by SMC with the premise of improving the handling stability. Although a few domestic and international scholars at home and abroad have tried to explore the performance of FSMC, they have focused mainly on the adaptive analysis of FSMC to date as the existence of fuzzy control can adjust the parameters of SMC, which considerably improves the adaptability to different working conditions [13]–[17]. FSMC not only has the previously mentioned advantages but also can substantially reduce the chattering phenomenon and the sudden change in control variable using fuzzy approximation algorithms, which provides a basis for the application of the control method in practical engineering. Moreover, most studies on DYC do not involve state estimation, and a few studies involve parameter state estimation but do not show the effect of estimation [11], [18].

Distributed drive electric vehicle (DDEV) is driven by four independently controlled hub motors. As the driving force of each wheel is independently controlled and has the characteristics of fast response and high control accuracy, it is suitable enough for the application of DYC to DDEV [19]–[21]. Based on the previous discussion, a hierarchical control strategy based on FSMC is proposed to reduce chattering and render DYC adaptive under different working conditions. The contribution of this paper can be summarized as follows: A novel noise-adaptive unscented Kalman filter (AUKF) based on a 7-DOF vehicle model is designed to estimate the sideslip angle, which provides parameters that are not easily measured in practice by a controller. An adaptive FSMC method is designed to calculate the additional yaw moment at the decision-making level, and a method based on the axle load ratio is established to distribute the yaw moment to four hub motors as the distribution layer to improve the handling stability of a DDEV under extreme conditions. The experimental data are obtained through the joint simulation of CarSim and MATLAB/Simulink, and the effectiveness of the FSMC control method established in this paper is analyzed in detail by comparing the control process and control results with SMC.

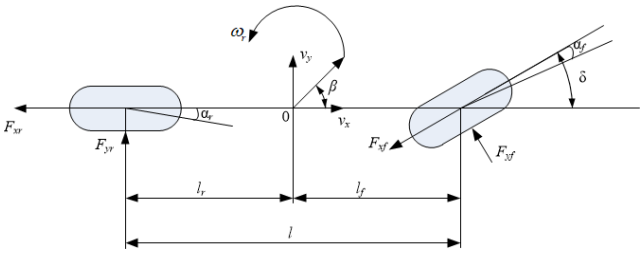

FIGURE 1. Vehicle Linear 2DOF Model.

The remainder of this paper is organized as follows: Section 2 introduces the two degrees of freedom vehicle model, seven degrees of freedom model, electric-driving wheel model and vehicle parameter setting. Section 3 presents the design process of the controller, including the estimation of the sideslip angle based on the AUKF, upper FSMC control method and the lower axle load proportion-based allocation method. Section 4 carries out joint simulation tests under two typical working conditions, compares FSMC, SMC and uncontrolled vehicles and analyses the results. Section 5 summarizes the research in this paper.

II. VEHICLE DYNAMIC MODEL

A. TWO DEGREES OF FREEDOM VEHICLE MODEL

A linear 2-DOF vehicle model is shown in Fig. 1. This model is a 2-DOF model with a front wheel rotation angle as the input, which is supported by front and rear tires with lateral elasticity on the ground, and possesses lateral and yaw motion.

The dynamic equation of body motion is expressed as follows:

$$\left(k_f+k_r\right)\beta+\frac{1}{v_x}\left(l_fk_f-l_rk_r\right)\omega_{\mathrm{r}}-k_f\delta=m\left(\dot{v}_y+v_x\omega_{\mathrm{r}}\right) \tag{1}$$

$$\left(l_fk_f-l_rk_r\right)\beta+\frac{1}{v_x}\left(l_f^2k_f+l_r^2k_r\right)\omega_{\mathrm{r}}-l_fk_f\delta=I_z\dot{\omega}_{\mathrm{r}} \tag{2}$$

The definitions and values of the variables in this formula and the whole article are shown in Table 1.

The model can characterize the relationship between the vehicle handling stability and the yaw rate and the sideslip angle. The 2DOF model represents the motion state of the vehicle in the ideal state; the calculated parameters will be used as the ideal reference value in this paper.

TABLE 1. Vehicle parameters.

Variable name	Meaning	Value
m	Vehicle mass	1240kg
l_f	Distance from center of mass to front axle	1157mm
l_r	Distance from center of mass to rear axle	1453mm
v_x/v_y	Longitude/Lateral velocity	m/s
k_f	Cornering stiffness of front tire	34820 N/rad
k_r	Cornering stiffness of rear tire	34820 N/rad
I_Z	Yaw moment of inertia	1662 kg.m^2
δ	Front wheel steering angle	deg
a_x	Longitudinal acceleration	m/s^2
B	Wheelbase	2610 mm
F_{zf}	Vertical load on front axle	N
F_{zr}	Vertical load on rear axle	N
h_g	Height of center of mass	510mm
r	Wheel rolling radius	307mm

In the steady state, the vehicle lateral acceleration is 0, the desired values of the yaw rate ωrd, and the sideslip angle βd can be deduced:

$$\omega_{rd} = \frac{v_x}{L + \frac{mv_x^2}{L}\left(\frac{l_f k_f - l_r k_r}{k_r k_f}\right)}\delta \tag{3}$$

$$\beta_d = \frac{2l_r\left(l_f + l_r\right)k_f k_r - mv_x^2 l_f k_f}{2l_r\left(l_f + l_r\right)^2 k_f k_r - mv_x^2\left(l_f k_f - l_r k_r\right)}\delta \tag{4}$$

The upper boundaries of the yaw rate and sideslip angle are related to the road surface, so the dynamic boundaries associated with the tire-road adhesion coefficient are constructed after obtaining the ideal expressions [22].

The lateral acceleration at the mass center can be written as:

$$a_y = \omega_r v_x + \dot{v}_y \tag{5}$$

After substituting $v_y = v_x \tan(\beta)$, the lateral acceleration can be expressed as:

$$a_y = v_x\omega_r + \tan(\beta)a_x + \frac{v_x\dot{\beta}}{\sqrt{1+\tan^2(\beta)}} \tag{6}$$

As can be seen from equation (6), both sideslip angle and yaw rate have effects on lateral acceleration, while the values of the last two terms are much smaller relative to the first term, the maximum yaw rate ω_{rdmax} can be obtained by combining $a_y \le \mu g$ and equation (6) according to experience [18], [23]:

$$\omega_{r\,\max} = 0.85\frac{\mu g}{v_x} \tag{7}$$

Then, a more reasonable expression of ideal yaw angular velocity can be obtained [24]:

$$\omega_{rdes} = \min\{|\omega_{rd}|, |\omega_{r\,\max}|\}\text{sgn}(\omega_{rd}) \tag{8}$$

The maximum sideslip angle is usually estimated by the following formula [25]:

$$\beta_{\max} = \arctan(0.02\mu g) \tag{9}$$

A more reasonable expression of the ideal sideslip angle can be obtained as follows:

$$\beta_{des} = \min\{|\beta_d|, |\beta_{\max}|\}\text{sgn}(\beta_d) \tag{10}$$

B. SEVEN DEGREES OF FREEDOM VEHICLE MODEL

The 7-DOF vehicle model includes the motion equations of the longitudinal, lateral, and yaw directions and the four wheels of the vehicle. Formula (11) ~ Formula (13) are the vehicle longitudinal motion equation, lateral motion equation and yaw motion equation, respectively. This model will be used to estimate the sideslip angle in this paper.

$$\begin{aligned} ma_x &= m(\dot{v}_x - \omega_r \cdot v_y) = (F_{xfl} + F_{xfr})\cos\delta \\ &\quad - (F_{yfl} + F_{yfr})\sin\delta + F_{xrl} + F_{xrr} \end{aligned} \tag{11}$$

$$\begin{aligned} ma_y &= m(\dot{v}_y + \omega_r \cdot v_x) = (F_{xfl} + F_{xfr})\sin\delta \\ &\quad + (F_{yfl} + F_{yfr})\cos\delta + F_{yrl} + F_{yrr} \end{aligned} \tag{12}$$

$$\begin{aligned} I_z \cdot \dot{\omega}_r &= [(F_{xfl} + F_{xfr})\sin\delta + (F_{yfl} + F_{yfr})\cos\delta]l_f \\ &\quad + [(F_{xfr} - F_{xfl})\cos\delta + (F_{yfl} - F_{yfr})\sin\delta]\frac{t_{w1}}{2} \\ &\quad + (F_{xrr} - F_{xrl})\frac{t_{w2}}{2} - (F_{yrl} + F_{yrr})l_r \end{aligned} \tag{13}$$

where δ are the steering angle of the front wheels, and vx and vy are the longitudinal vehicle speed and lateral vehicle speed, respectively. F_{xi}, F_{yi} and F_{zi} are the tire longitudinal force, lateral force and vertical force, respectively, and tw1 and tw2 are the treads of the front wheels and rear wheels, respectively.

C. ELECTRIC-DRIVING WHEEL MODEL

A DDEV uses four hub motors instead of a traditional internal combustion engine as the power output, which is an important part of an electric-wheeled vehicle. As the main research content of this paper is the method of controlling the direct yaw moment, and the motor control technology is currently relatively mature, this paper does not focus on the performance of motor control but simplifies the electromagnetic conversion process of the motor into a second-order transfer function mathematical model [26]:

$$G(s) = \frac{T_{mi}}{T_{mdi}} = \frac{1}{2\xi^2 s^2 + 2\xi s + 1} \tag{14}$$

where T_{mi} represents the actual torque value of each hub motor, T_{mdi} represents the expected torque value of each hub motor and ζ represents the damping ratio that is related to the parameters of the hub motor.

Calculating tire longitudinal force F_{xi} by using the moment balance equation of four wheels:

$$I_{tw} \cdot \dot{\omega}_i = -r \cdot F_{xi} + T_i \tag{15}$$

where I_{tw} is the wheel moment of inertia. Besides the contribution of DYC, the specific value of T_i varies with the demand output of CarSim. ω_i is the angular speed of each wheel.

D. VEHICLE PARAMETER SETTING

A DDEV is driven by motors placed in the rim; thus, hub motors and tires are regarded as non-spring masses.

The parameters of a certain type of electric vehicle are also modified, as shown in Table 1 above.

CarSim software only has the model parameters of a traditional vehicle transmission system, the application object of this paper is a four-wheel drive electric vehicle, and four-wheel power is derived from the hub motor. Therefore, a traditional vehicle model in CarSim must be modified to obtain the transmission characteristics of DDEV. First, the power transmission system of the original vehicle model is interrupted and changed to a four-wheel drive mode. The output torque of the motor is directly loaded on the wheel. The numerical value is calculated by the proposed control method and outputted to the CarSim vehicle model.

III. CONTROLLER DESIGN

The completion of DYC requires two parts [27]. First, the core decision-making layer calculates the additional yaw moment according to the deviation between the yaw rate, sideslip angle and their corresponding ideal values. Second, the yaw moment calculated by the decision-making layer is distributed to the hub motor of four wheels under the control of the distribution layer, and the yaw moment is realized by the longitudinal force difference between the wheels on both sides. The sideslip angle required by the controller is difficult to accurately measure using sensors. Therefore, the AUKF is used to estimate the sideslip angle for subsequent control.

A. ESTIMATION OF SIDESLIP ANGLE

According to the definition of the sideslip angle, the estimation of the sideslip angle requires the estimation of the longitudinal and lateral speeds, and then is calculated by formula 16 [28]. The vehicle model has an important role in the accuracy of speed estimation. Therefore, based on the 7DOF vehicle model mentioned above, a noise-adaptive unscented Kalman filter is used to estimate the vehicle speed.

$$\beta = \arctan(\frac{v_y}{v_x}) \tag{16}$$

According to the dynamic equation, the longitudinal acceleration a_x and lateral acceleration a_y can be calculated by the following formula [29], [30]:

$$\begin{aligned} a_x &= (\dot{v}_x - \omega_r \cdot v_y) = [(F_{xfl} + F_{xfr})\cos\delta \\ &\quad - (F_{yfl} + F_{yfr})\sin\delta + F_{xrl} + F_{xrr}]/m \end{aligned} \tag{17}$$

$$\begin{aligned} a_y &= (\dot{v}_y + \omega_r \cdot v_x) = [(F_{xfl} + F_{xfr})\sin\delta \\ &\quad + (F_{yfl} + F_{yfr})\cos\delta + F_{yrl} + F_{yrr}]/m \end{aligned} \tag{18}$$

The longitudinal force F_{xi} of the wheel can be obtained by the moment balance equation in equation (15), and the lateral force can be obtained by the dug off tire model. The key tire parameters of longitudinal stiffness C_x and lateral stiffness C_y are mainly related to the vertical load. By interpolation of CarSim's tire test data, the corresponding values under an arbitrary vertical load can be obtained. The data table is encapsulated by the "lookup table" module in Simulink; the longitudinal stiffness and the lateral stiffness are invoked by the longitudinal slip rate and the sideslip angle of tire, respectively. Some of the data at a sideslip angle of 0.174 rad and a slip rate of 0.2 are shown in the following table.

TABLE 2. Partial values of tire longitudinal stiffness and lateral stiffness under different vertical loads.

Vertical load(N)	1593.58	3187.16	4780.74	6374.32	7967.9
C_x(N/m)	7877	15574	23060	30317	37331
C_y(N/rad)	9066	17932	26564	34939	43040

The state equation and observation equation of the nonlinear system are established according to the previous equation of vehicle motion as follows:

$$\begin{pmatrix} v_x \\ v_y \\ \omega_r \end{pmatrix}_k = \begin{pmatrix} v_x \\ v_y \\ \omega_r \end{pmatrix}_{k-1} + \begin{pmatrix} \dot{v}_x \\ \dot{v}_y \\ \dot{\omega}_r \end{pmatrix} \cdot t + w(t) \tag{19}$$

$$\begin{pmatrix} a_x \\ a_y \\ \omega_r \end{pmatrix}_k = \begin{pmatrix} [(F_{xfl}+F_{xfr})\cos\delta - (F_{yfl}+F_{yfr})\sin\delta + F_{xrl} + F_{xrr}]/m \\ [(F_{xfl}+F_{xfr})\sin\delta + (F_{yfl}+F_{yfr})\cos\delta + F_{yrl} + F_{yrr}]/m \\ \omega_r \end{pmatrix}_k + v(t) \tag{20}$$

Choose the state vector $x = (v_y v_x \omega_r)^{\mathrm{T}}$, the measurement vector $y = (a_y a_x \omega_r)^{\mathrm{T}}$, and the input variable $u = (\delta T_{ij} \omega_{ij})$. w(t) and v(t) are the process noise and the observation noise, respectively; assuming they are independent white Gaussian noise, the mean values are q_k and r_k, respectively, and the covariances are Q_k and R_k respectively. The measurement noise covariance R_k is usually calculated by the system observation value obtained by the sensor, which can be regarded as a known quantity. Due to the process signal cannot be observed directly, it is usually more difficult to determine the value of the process excitation noise covariance Q_k. Therefore, this paper designs a special Q_k which adaptively changes with the uncertainty of the model.

The AUKF algorithm is designed after the state equation and measurement equation are determined. The core idea of the noise-adaptive unscented Kalman algorithm is to dynamically estimate the statistical characteristics of system noise in real time using the data of the measurement variables in the filtering process. The estimated noise parameters are used to estimate the state parameters of the UKF, and the state estimates of the system are continuously and iteratively obtained under various conditions. Compared with EKF, the improved UKF has the following advantages: (1) The estimation accuracy is higher than that of EKF. Approximating the probability density distribution of the non-linear function, rather than linearizing the non-linear function. (2) The Jacobian matrix does not need to be computed by derivation, which improves

the computational speed. (3) It can deal with random noise and discrete systems, and expands the application scope. (4) The process noise covariance Qk adaptively adjusted by the following model uncertainty makes AUKF have good estimation performance under different conditions.

The flow chart of the estimation algorithm is described as follows [31]:

1) UT transformation. Using a symmetrical sampling strategy, 2N+1 sigma point set is obtained near each estimation point.

$$x(k-1) = [\hat{x}(k-1)\hat{x}(k-1) + \sqrt{(N+\lambda)\cdot P_i(k-1)} \times \hat{x}(k-1) - \sqrt{(N+\lambda)\cdot P_i(k-1)}] \quad (21)$$

where $i = 1, 2\ldots, \mathrm{N}$. λ is a proportional parameter, and N is the dimension of the state vector x.

2) Prediction process. Nonlinear transformation of a sigma point set is carried out by using the nonlinear state equation of the estimation model, and the predicted state mean at the current time is obtained by UT mean weighting calculation.

$$\begin{cases} x(k|k-1) = f(x(k-1), u(k-1)) \\ \hat{x}(k|k-1) = \sum_{i=0}^{2N} W_i^{(m)} x_i(k|k-1) \end{cases} \quad (22)$$

where $x_{\mathrm{i}}(\mathrm{k}|\mathrm{k}-1)$ represents the i-th column of matrix $x(\mathrm{k}|\mathrm{k}-1)$.

The predicted state variance of the current time is obtained by the weighting UT variance by means of the predicted state mean of the current time:

$$P(k|k-1) = \sum_{i=0}^{2N} W_i^{(c)} (x_i(k|k-1) - \hat{x}(k|k-1)) \cdot (x_i(k|k-1) - \hat{x}(k|k-1))^T + Q_k \quad (23)$$

Each sigma point is nonlinearly transformed using the observation equation:

$$\varsigma(k|k-1) = h(x(k|k-1), u(k-1)) \quad (24)$$

The weighted sum of the changed point sets is used to calculate the predicted observations of the system.

$$\hat{y}(k|k-1) = \sum_{i=0}^{2N} W_i^{(m)} \varsigma_i(k|k-1) \quad (25)$$

where $\varsigma_i(k|k-1)$ represents the i-th column of the matrix $\varsigma(k|k-1)$.

3) Updating process.

Update the system variance matrix:

$$P_{yy} = \sum_{i=0}^{2N} W_i^{(c)} (\varsigma_i(k|k-1) - \hat{y}(k|k-1)) \cdot (\varsigma_i(k|k-1) - \hat{y}(k|k-1))^T + R_k \quad (26)$$

Update the cross-correlation covariance matrix:

$$P_{xy} = \sum_{i=0}^{2N} W_i^{(c)} (x_i(k|k-1) - \hat{x}(k|k-1)) \cdot (\varsigma_i(k|k-1) - \hat{y}(k|k-1))^T \quad (27)$$

Update the filter gain matrix:

$$K(k) = P_{xy}(k|k-1) P_{yy}^{-1}(k|k-1) \quad (28)$$

Estimate the values after the status updates:

$$\hat{x}(k|k) = \hat{x}(k|k-1) + K(k)(y(k) - \hat{y}(k|k-1)) \quad (29)$$

Calculate the state posterior variance matrix:

$$P(k|k) = P(k|k-1) - K(k) P_{yy} K^T(k) \quad (30)$$

4) Noise statistical characteristics update:

$$\begin{cases} \hat{q}_k = (1-d_k)\hat{q}_{k-1} + d_k(\hat{x}(k|k) - \hat{x}(k|k-1)) \\ \hat{Q}_k = (1-d_k)\hat{Q}_{k-1} + d_k\,[K(k)(y(k) - \hat{y}(k|k-1)) \\ \cdot (y(k) - \hat{y}(k|k-1))^T K^T(k) + P(k|k) - P_{xy}] \end{cases} \quad (31)$$

where $\mathrm{d_k} = (1-\mathrm{b})/(1-\mathrm{b}^{\mathrm{k}+1})$, and b is a forgetting factor. In this paper, formula (31) is introduced in the AUKF, the noise of a stochastic system is estimated after state updating, and the next prediction is made. Thus, the noise adaptive UKF is constructed by the cycle.

B. ADAPTIVE FUZZY SLIDING MODE CONTROLLER

The controller is designed after all parameters are ready. The selection of a sliding surface should not only satisfy the trajectory of the yaw rate but also consider the trajectory of the sideslip angle. From the motion equation of the linear two-degree-of-freedom vehicle model, the yaw rate ωr and the sideslip angle β have a certain coupling relationship, and one variable alone cannot fully reflect the state of vehicle motion. Therefore, the joint control of ωr and β is analyzed in this paper. The design of sliding mode control is mainly divided into the design of a sliding mode surface and the choice of reaching law. When these two points are determined, the expression of the control variable can be derived.

First, the sliding surface is defined as follows:

$$s = \varepsilon\,(\omega_r - \omega_{rdes}) + \xi\,(\beta - \beta_{des}) \quad (32)$$

Second, the differential on both sides of equation (12) is obtained:

$$\dot{s} = \varepsilon\,(\dot{\omega}_r - \dot{\omega}_{rdes}) + \xi\,\left(\dot{\beta} - \dot{\beta}_{des}\right) \quad (33)$$

After adding an additional yaw moment, formula (2) is rewritten as follows [32]:

$$\left(l_f K_f - l_r K_r\right)\beta - I_z\dot{\omega}_r + \frac{\left(l_f^2 K_f + l_r^2 K_r\right)}{V_x}\omega_r + \Delta M = l_f K_f \delta \quad (34)$$

$\dot{\omega}_r$ in formula (34) is expressed by other quantities and substituted into formula (33) and sorted out.

$$\Delta M = -\frac{I}{\varepsilon}\dot{s} - \left(l_f K_f - l_r K_r\right)\beta - \frac{\left(l_f^2 K_f + l_r^2 K_r\right)}{V}\omega_r + l_f K_f \delta - I\dot{\omega}_{rdes} + \frac{I\xi}{\varepsilon}\left(\dot{\beta} - \dot{\beta}_{des}\right) \quad (35)$$

In this paper, the exponential reaching law is chosen to restrict the trajectory of the system:

$$\dot{s} = -k \operatorname{sgn} s - bs \tag{36}$$

Substitute Formula (36) into Formula (35) and obtain the following formula:

$$\begin{aligned}\Delta M = &-\frac{I}{\varepsilon}(-k \operatorname{sgn} s - bs) - \left(l_f K_f - l_r K_r\right)\beta \\ &- \frac{\left(l_f^2 K_f + l_r^2 K_r\right)}{V}\omega_r + l_f K_f \delta - I\dot{\omega}_{rdes} \\ &+ \frac{I\xi}{\varepsilon}\left(\dot{\beta} - \dot{\beta}_{des}\right)\end{aligned} \tag{37}$$

Finally, the stability of the system using Formula (36) as the control law is analyzed. The stability is proven as follows:

Consider the Lyapunov function as follows:

$$V = \frac{1}{2}s^2 \tag{38}$$

By substituting the control law of Formula (36), we can obtain:

$$\dot{V} = s\dot{s} = s(-k \operatorname{sgn} s - bs) = -k|s| - bs^2 < 0 \tag{39}$$

According to formula (37), the existence of symbolic functions can effectively eliminate the unknown interference terms, while inevitably leading to chattering. Therefore, this paper adopts a fuzzy approximation algorithm to construct continuous of discrete symbolic functions; thus, the chattering phenomenon can be fundamentally reduced. The design process of the fuzzy approximation is described below.

The product inference engine, single-valued ambiguity and central average ambiguity resolver are employed. The output y(x) of a fuzzy system can be written as follows:

$$y(\mathrm{x}) = \frac{\sum_{j=1}^{m} y^j (\prod_{i=1}^{n} \mu_{A_i^j(x_i)})}{\sum_{j=1}^{m} (\prod_{i=1}^{n} \mu_{A_i^j(x_i)})} \tag{40}$$

The switching function s(t) is taken as the input of the fuzzy system, where A_1^j is its fuzzy set {NB NS ZO PS PB}, and $\mu_{A_i^j(\mathrm{s}_i)}$ is the membership function of s_i:

$$\begin{aligned}\mu_{NB}(s) &= \frac{1}{1+\exp(5(s+4))}, \\ \mu_{NS}(s) &= \frac{1}{1+\exp(5(s+2))}, \\ \mu_{ZO(s)} &= \exp(-s^2), \\ \mu_{PS}(s) &= \frac{1}{1+\exp(5(s-2))}, \\ \mu_{PB}(s) &= \frac{1}{1+\exp(5(s-4))}.\end{aligned}$$

The following fuzzy system $\hat{h}(S, \hat{\theta})$ is employed as the output to continuous approach $(k/\varepsilon)\mathrm{sgn}s$:

$$\hat{h}(s|\hat{\theta}) = \hat{\theta}^T \phi(s) \tag{41}$$

$\phi(s)$ is a fuzzy vector satisfy the form $\frac{(\prod_{i=1}^{n} \mu_{A_i^j(s_i)})}{\sum_{j=1}^{m}(\prod_{i=1}^{n} \mu_{A_i^j(s_i)})}$, θ^T is the degree of adjustment, which varies according to the adaptive law. In the ideal state $\hat{h}(s|\hat{\theta}) = \frac{k}{\varepsilon}sgns$, while the actual driving conditions are complex and changeable, the ideal state cannot be ensured for a long time. To generate $\hat{h}(S, \hat{\theta})$ in real time and make it infinitely approach $(k/\varepsilon)\mathrm{sgn}s$, the following adaptive laws are designed to adjust $\hat{\theta}$:

$$\dot{\hat{\theta}} = rs\phi(s) \tag{42}$$

where r is a normal number, and the setting is designed according to the system state. The optimal adjustment parameter $\hat{\theta}^*$ is determined by formula (43). Thus, $\phi(s)$ should be adjusted in real time with a change in $s(t)$. The objective is to minimize the adjustment error $e_\theta = \dot{\hat{\theta}} - \hat{\theta}^*$.

$$\hat{\theta}^* = \arg\min_{\theta \in \Omega}[\sup|\hat{h}(s|\hat{\theta}) - \frac{k}{\varepsilon}\operatorname{sgn} s] \tag{43}$$

where Ω is the set of θ.

After introducing $\hat{h}$, formula (37) can be rewritten as:

$$\begin{aligned}\Delta M = &\frac{I\mathrm{b}}{\varepsilon}s - \left(l_f K_f - l_r K_r\right)\beta - \frac{\left(l_f^2 K_f + l_r^2 K_r\right)}{V}\omega_r \\ &+ l_f K_f \delta - I\dot{\omega}_{rdes} + \frac{I\xi}{\varepsilon}\left(\dot{\beta} - \dot{\beta}_{des}\right) + \hat{h}(S, \hat{\theta})\end{aligned} \tag{44}$$

When the switching term is continuous, the coefficient k of $\frac{k}{\varepsilon}\operatorname{sgn} s$ should be able to change with the motion state of the system, so as to make the approximated fuzzy system $\hat{h}(S, \hat{\theta})$ have a higher condition adaptability.

Therefore, a variable switching gain is designed, and the switching gain is adjusted according to the relative position, the movement trend of the system and the sliding surface by using the fuzzy rules. $s\dot{s}$ is regarded as the fuzzy input, k is regarded as the output, the parameters $s\dot{s}$ and k are transformed into the fuzzy sets of s[−2, 2] and k[−2, 2], respectively, and the corresponding fuzzy linguistic variables are $s\dot{s}$ = {NB NM NS ZO PS PM PB}, and Δk = {NB NM NS ZO PS PM PB}. $s\dot{s} > 0$ indicates that the current state of the sliding mode function is the same as the change trend, and the sliding mode surface tends to be far from the sliding mode surface. The switching gain k should be increased at that time. $s\dot{s}$ <0 indicates that the state of the sliding mode function is opposite of the changing trend at this time, the system is approaching the sliding mode surface, and the switching gain k should be reduced. However, the size of $|s\dot{s}|$ also needs to be considered to further rationalize the design of the fuzzy rules. When $|s\dot{s}|$ is large, $|k|$ should also undergo a larger change, and vice versa. Based on this analysis, the membership function diagram of the fuzzy rules and the fuzzy system can be obtained.

In the design of the fuzzy controller, the design of the fuzzy rules is an important link for determining its performance. In this paper, seven fuzzy rules for the switching gain coefficient k are detailed as follows:

R1: IF $s\dot{s}$ is PB THEN Δk is PB;
R2: IF $s\dot{s}$ is PM THEN Δk is PM;
R3: IF $s\dot{s}$ is PS THEN Δk is PS;
R4: IF $s\dot{s}$ is ZO THEN Δk is ZO;
R5: IF $s\dot{s}$ is NS THEN Δk is NS;
R6: IF $s\dot{s}$ is NM THEN Δk is NM;
R7: IF $s\dot{s}$ is NB THEN Δk is NB.

The designed adaptive fuzzy sliding mode controller enables the fuzzy system $\hat{h}(S, \hat{\theta})$ to approximate the symbolic function with variable gain in real time and reduce chattering with the premise of self-adaptation.

C. TORQUE DISTRIBUTION CONTROLLER

In this paper, the axle load proportional distribution algorithm is used to distribute the four-wheel driving force according to the vertical load on front and rear vehicle axles. This method should satisfy not only the additional yaw moment but also the longitudinal force requirement of a vehicle [33].

The methods for determining the estimated values of front and rear axle loads are presented as follows:

$$\begin{cases} F_{zf} = \dfrac{mgl_r - a_x \cdot h_g}{L} \\ F_{zr} = \dfrac{mgl_f + a_x \cdot h_g}{L} \end{cases} \tag{45}$$

When the DDEV distributes the longitudinal force of each wheel using the axle load proportional distribution algorithm, the longitudinal force of each wheel must satisfy the requirements of the longitudinal force and additional yaw moment, as well as the following formula [28]:

$$\begin{cases} \dfrac{F_{x1} + F_{x3}}{F_{zf}} = \dfrac{F_{x2} + F_{x4}}{F_{zr}} \\ \dfrac{F_{x3} - F_{x1}}{F_{zf}} = \dfrac{F_{x4} - F_{x2}}{F_{zr}} \end{cases} \tag{46}$$

From the vehicle kinematics, the longitudinal force of four wheels is obtained as follows:

$$\begin{cases} F_{x1} = \dfrac{mgl_r - a_x \cdot h_g}{2mgL} \left(\dfrac{\sum F_x}{2} - \dfrac{\sum M}{B/2} \right) \\ F_{x2} = \dfrac{mgl_f + a_x \cdot h_g}{2mgL} \left(\dfrac{\sum F_x}{2} - \dfrac{\sum M}{B/2} \right) \\ F_{x3} = \dfrac{mgl_r - a_x \cdot h_g}{2mgL} \left(\dfrac{\sum F_x}{2} + \dfrac{\sum M}{B/2} \right) \\ F_{x4} = \dfrac{mgl_f + a_x \cdot h_g}{2mgL} \left(\dfrac{\sum F_x}{2} + \dfrac{\sum M}{B/2} \right) \end{cases} \tag{47}$$

The optimized four-wheel longitudinal force of the DDEV can be obtained by considering the road adhesion limit:

$$|F_{xi}| \leq \min\left(F_{xi}, \mu F_{zi}\right), \quad i = 1, 2, 3, 4 \tag{48}$$

According to the tire radius, the longitudinal force of each wheel is converted to the required output torque T_i of the hub motor, which is outputted to equation (15) and CarSim from the motor model.

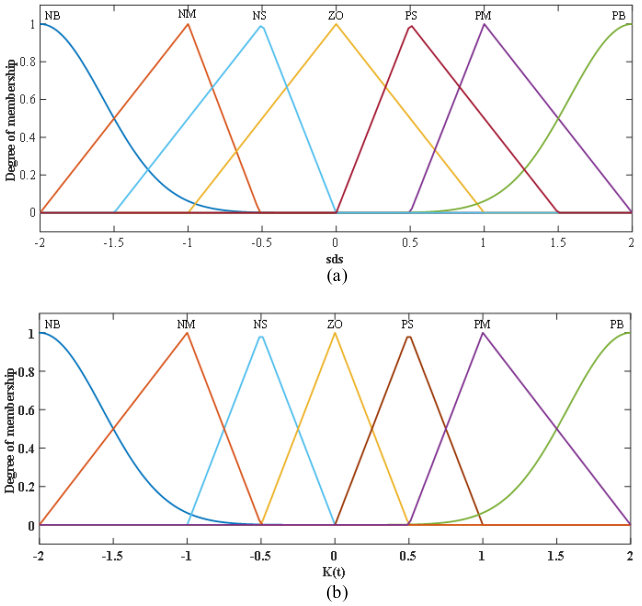

FIGURE 2. (a) Membership function of switching gain coefficient K(t). (b). Membership function of the product of sliding mode surface function s and its derivative ṡ.

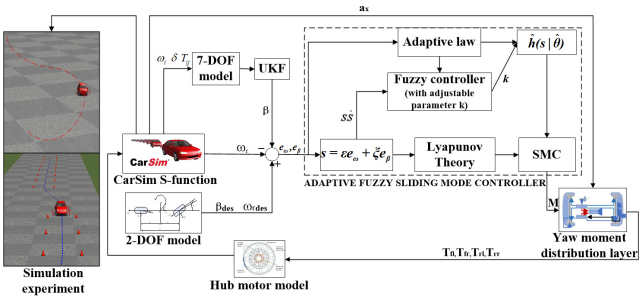

FIGURE 3. The overall architecture layout of the simulation validation test.

IV. RESULTS AND DISCUSSION

To verify the effect of the previous work, CarSim is used to carry out the simulation test because of the lack of necessary real-lane experimental conditions and the danger of this test. In this paper, the Simulink model of FSMC, and the whole vehicle model in CarSim are used to carry out joint simulation tests under two working conditions, which include a double lane-shifting test and fishhook test, the estimation effect of AUKF is verified under two conditions, and the traditional SMC and unstable control are compared with the FSMC designed. The overall layout is shown in Fig. 3 [34], [35].

A. DOUBLE LANE SHIFT TEST

The double lane change test, which is also known as the elk test, aims to simulate the ability of a vehicle to quickly steer and recover the original lane after urgently avoiding obstacles [37]. Specific parameters are established as follows:

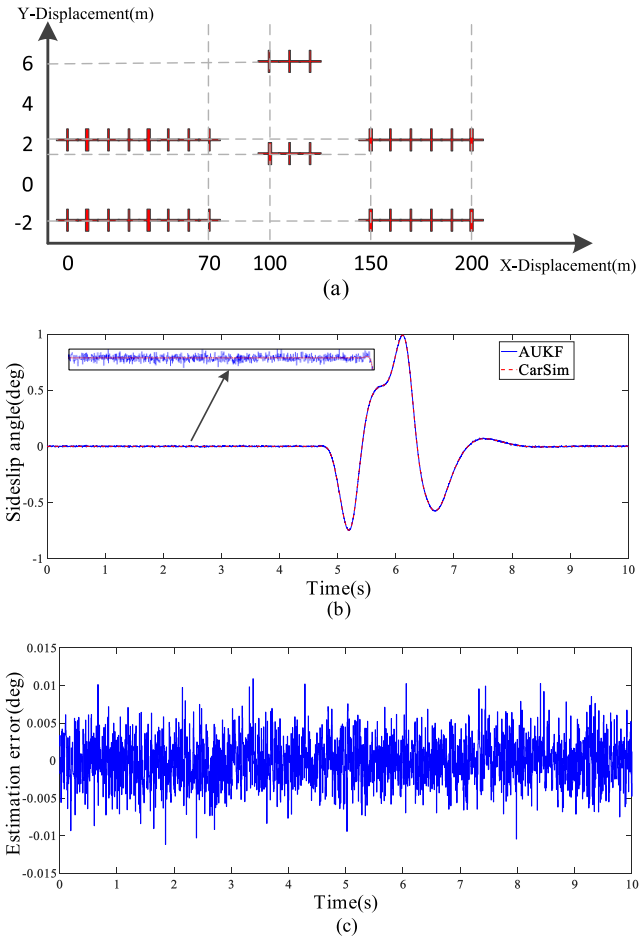

FIGURE 4. (a). DLC test Lane layout. (b). Comparison of estimated sideslip angle and real value. (c). Sideslip angle estimation error.

the vehicle speed is 80 km/h, road adhesion coefficient is 0.5, and test lane layout is shown in Fig. 4. (a).

The AUKF designed in this paper can estimate the sideslip angle as shown in Fig. 4(b). To strictly ensure that the input variables (sideslip angle) of CarSim are always at the same frequency as the calculated variables (sideslip angle) of AUKF estimator, Simulink is set to a fixed step size in simulation, and its sampling time corresponds to the output period setting in CarSim, so as to ensure the real-time performance in calculating yaw moment. As the CarSim software is based on the data obtained from the exact test, the sideslip angle generated by the CarSim software is taken as the true value. As shown in Fig. 4(c), the error range of the AUKF estimation method is ± 0.01 deg, which has a fairly high estimation accuracy. Therefore, the follow-up research has practical significance.

The additional yaw moments obtained by the traditional SMC control method and the FSMC control method are shown in Fig. 5. (a) and Fig. 5. (b), respectively. The SMC control method has a continuous large-scale chattering phenomenon in the range of 0-2 seconds and 6.6-6.8 seconds, and the amplitude is approximately ± 200 N·m. However, the additional yaw moment calculated by FSMC has a sudden

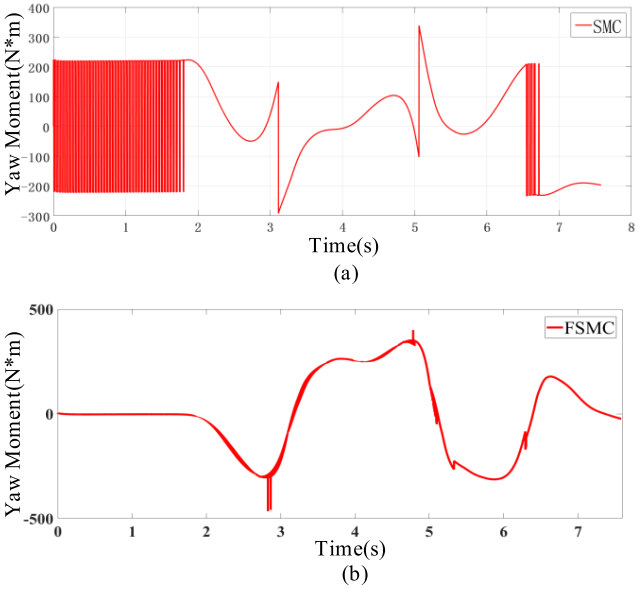

FIGURE 5. (a). Yaw moment in SMC control mode. (b). Yaw moment in FSMC control mode.

change of 177.194 N·m in 2.8299 seconds and 180.3 N·m in 2.8669 seconds. No other large, sudden changes occur in the whole test, and only a few small sudden changes and buffeting occur. From the transient response of yaw moment, the former has a sudden change in the opposite direction of expected control at the time when accidents are more likely to occur. Conversely, although sudden changes occur in the control variable of FSMC at the critical point of bending, the amplitude of FSMC distinctly decreases and the subsequent control quickly returns to normal.

According to the results, it can be inferred that the required yaw moment calculated by the SMC method will produce distinct chattering, and the tracking control ability is poor when the system motion state sharply changes. The reason may be that the motion state of the vehicle substantially changes before and after turning, and the control moment should decrease after bending, while the traditional SMC cannot adequately adjust the change rate. In addition. SMC is sensitive to interference before reaching the sliding mode surface, which causes a large instantaneous sudden change when the vehicle crosses the curve.

After calculating the required yaw moment, it is allocated to four hub motors, and the required yaw moment is achieved by controlling the differential speed of each wheel. Motor torques that correspond to the four wheels under the control of SMC and FSMC are shown in Fig. 6.(a) and Fig. 6.(b). Due to the chattering and abrupt change of the SMC method for calculating the required yaw moment, the executing mechanism will also have corresponding problems. The sudden change in torque chattering not only affects the comfort of the vehicle but also causes substantial damage to the motor and other components, which considerably shortens its life. The time-varying curve of the four-wheel motor torque controlled by

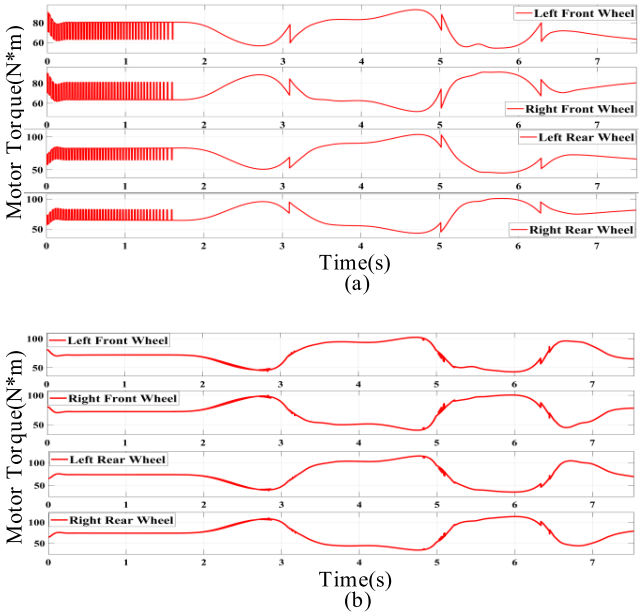

FIGURE 6. (a). Output torque of hub motor in SMC control mode. (b). Output torque of hub motor in FSMC control mode.

TABLE 3. Output torque chattering amplitude of left front wheel hub motor under DLC.

Time (s)	SMC (N·m)	FSMC (N·m)	Reduced (%)
Average (0-1.5)	17.8082	< 0.02	99.88
Average (3-3.2)	2.3230	< 0.02	99.14
Average (4.9-5.3)	2.6470	0.1136	95.71
Max (0-8)	17.8878	3.6374	79.67

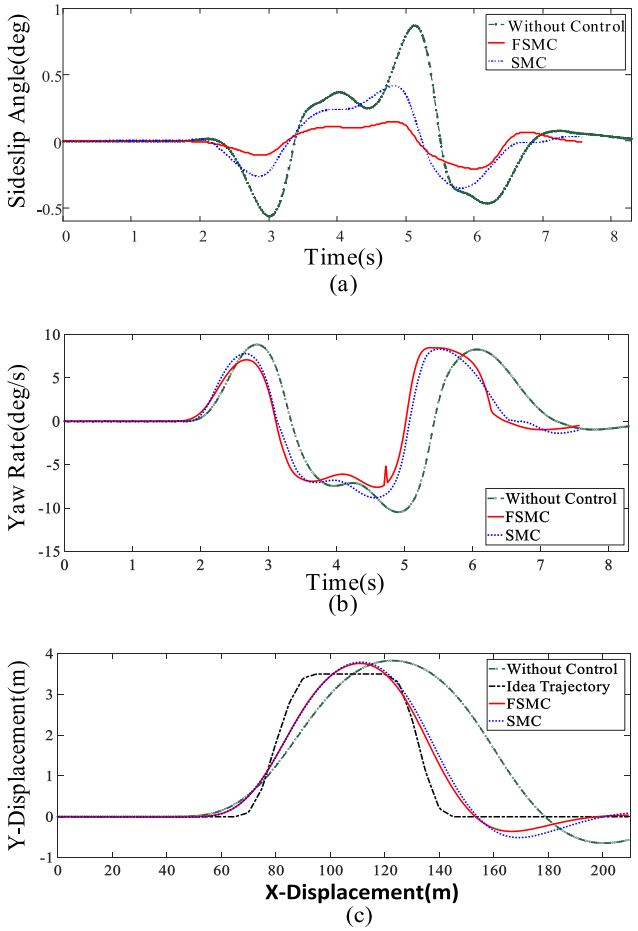

FIGURE 7. (a). Response curve of sideslip angle under double lane shifting condition. (b). Response curve of yaw rate under double lane shift conditions. (c). Vehicle trajectory under double lane change condition.

the FSMC method is consistent with the yaw moment waveform, and only small buffeting occurs in a limited amount of time. Compared with traditional SMC, both the amplitude and frequency of buffeting are substantially reduced. Taking the left front wheel as an example, a comparison of the buffeting amplitude is shown in Table 3.

After analyzing the advantages and disadvantages of the two methods in the control process, the control effect is compared according to Fig. 7. (a)-(c). As shown in Fig. 7. (a), the vehicle with the FSMC method can control the sideslip angle in the range of $-0.2°$ to $+0.15°$. Although the traditional SMC has reduced the range of the sideslip angle compared with the vehicle without control, a large deviation remains from 5-6 seconds of the test with a maximum value of $-0.35°$, which represents the tendency of the vehicle to slip or even rollover at this time. In terms of the yaw rate, the traditional SMC method and FSMC method have a better control effect, which renders the yaw rate follow-up response faster and controlled within the range of ± 10 deg/s. However, the SMC method is not as reliable as the FSMC method, and the yaw rate of the test vehicle is even greater than that of the uncontrolled vehicle from 4-5 seconds. From the point of view of the trajectory, FSMC has the best control effect, and is the first one to attain the predetermined trajectory when the test of double lane change is almost completed. The maximum offset in the Y direction is less than the other two methods, while uncontrolled vehicles have basically lost control.

The FSMC method can adequately limit the sideslip angle and yaw rate to a small range in the whole process, which not only guarantees safety but also improves the comfort. The inappropriate calculation of an additional yaw moment in the SMC method generates a steep increase of yaw rate from 4-5 seconds, which may make passengers more uncomfortable than that without control in some cases. Therefore, excellent adaptability is important. The yaw rate and sideslip curve of FSMC and SMC stop after 7.5 seconds because the vehicle has completed the test first, while the uncontrolled vehicle greatly deviates from the predetermined trajectory, which produces a longer test time.

B. FISHHOOK TEST

The fishhook test is a high-speed collision avoidance test, which is a common test for testing an electronic active safety control system. This test can fully verify the function of vehicles in a nonlinear area. The simulation results are detailed

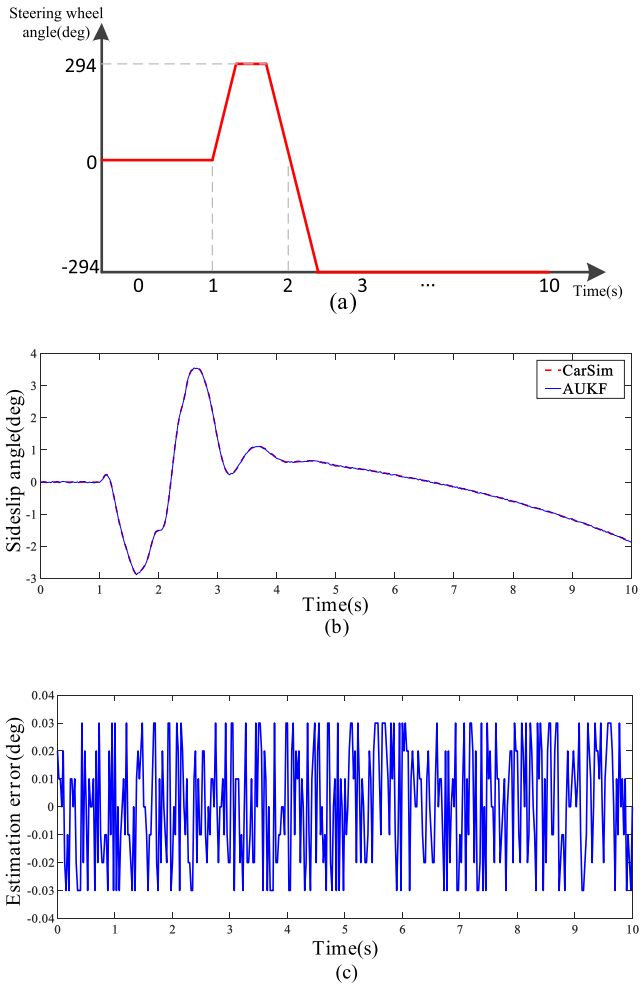

FIGURE 8. (a). Fishhook test steering wheel angle input. (b). Comparison of estimated sideslip angle and real value. (c). Sideslip angle estimation error.

as follows: the vehicle speed is 80 km/h, the road adhesion coefficient is 0.7, and the steering wheel angle input is shown in Fig. 8. (a) [37].

The estimated effect of the AUKF designed in this paper under the fishhook test condition is shown in Fig. 8 (b). The error range of the AUKF estimation method is basically between ±0.03 deg, although the error is larger than that of the DLC condition. Considering the larger value of the side slip angle under this condition, it can be considered to have a higher accuracy, and the follow-up research based on this finding has practical significance.

Fig. 9 shows that the yaw moment calculated by the SMC control method will have frequent buffeting when the vehicle's motion state rapidly changes, with an average amplitude of 187 N m, while the yaw moment calculated by FSMC has no buffeting. The yaw moment value obtained by the FSMC control method is larger, and the average value is 1176.45 N·m, while that of the SMC control method is 838.17 N m.

The control variable of FSMC under this condition is significantly higher than that of SMC. As the system will adjust

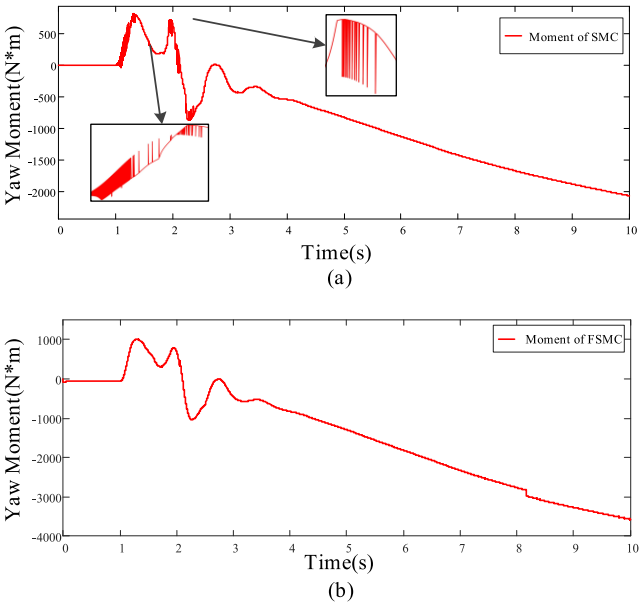

FIGURE 9. (a). Yaw moment in SMC control mode. (b). Yaw moment in FSMC control mode.

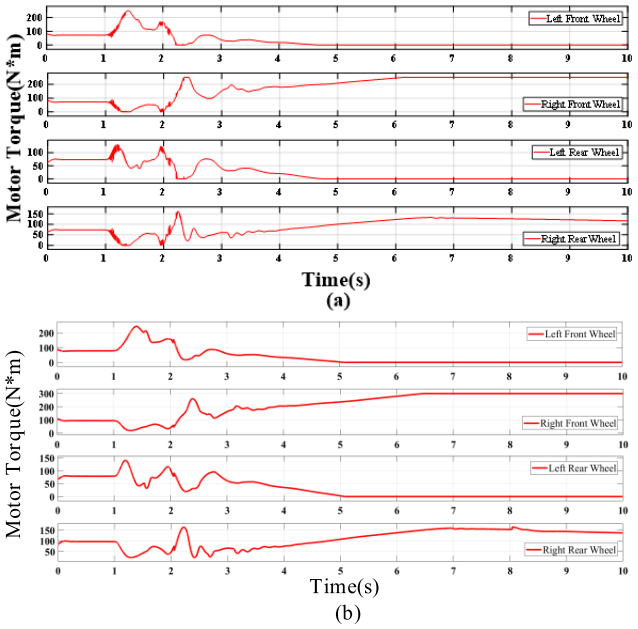

FIGURE 10. (a). Output torque of hub motor in SMC control mode. (b). Output torque of hub motor in FSMC control mode.

the switching gain coefficient according to the vehicle motion state, the subsequent control can be completed by the active adjustment coefficient when the instability tendency is large. Once the traditional SMC is designed, the coefficient cannot be changed, and the coefficient cannot be automatically adjusted according to the motion state.

As shown in Fig. 10, as the distribution of the motor torque must ensure the realization of the calculated yaw moment, the fluctuation of the yaw moment causes frequent chattering of the output torque of the hub motor, which will shorten the service life of motor and other electrical components for a

TABLE 4. Output torque chattering amplitude of left front wheel hub motor under fishhook.

Time (s)	SMC (N·m)	FSMC (N·m)	Reduced (%)
Average (1-1.5)	18.7179	<0.02	99.90
Average (2-2.5)	7.7974	<0.02	99.74
Max (0-10)	102.5582	22.6623	77.90
Average (1-1.5)	18.7179	<0.02	99.90

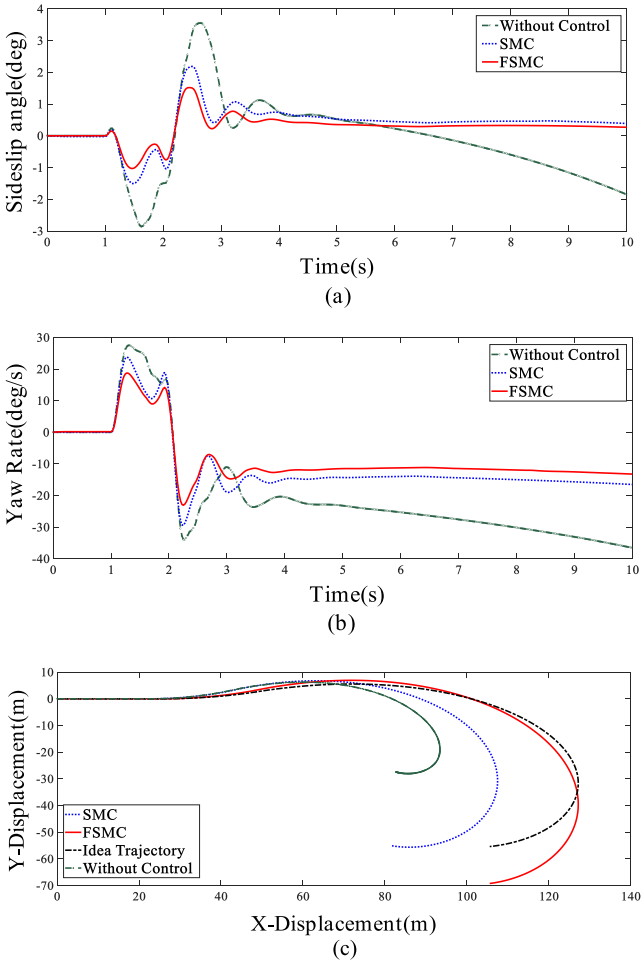

FIGURE 11. (a). Response curve of side slip angle under fishhook test condition. (b). Response curve of yaw rate under fishhook test condition. (c). Vehicle trajectories under fishhook test condition.

long time. Taking the left front wheel as an example, a comparison of the buffeting amplitude is shown in Table 4. The FSMC control method can substantially weaken the buffeting amplitude.

The differences among FSMC, SMC and uncontrolled vehicles are compared based on the control effect. The sideslip angle, yaw angular velocity and trajectory of FSMC, SMC and uncontrolled vehicles are shown in Fig. 11. The vehicle controlled by FSMC limits the sideslip angle from $-1°$ to $1.5°$, and the average absolute value of the sideslip angle is $0.382°$, which is less than $0.563°$ of the SMC control method. The yaw rate curve shows that the uncontrolled vehicle loses control after 3 seconds, and the rear axle side slip causes the vehicle yaw rate to increase. The yaw rate of an uncontrolled vehicle and a vehicle controlled by the SMC method is larger in 1-3 seconds, and a considerable yaw rate change rate exists before and after 2 seconds, which is 143.344 deg/s^2 and 64.738 deg/s^2, respectively. The FSMC control method designed in this paper restricts the occurrence of a large yaw rate and sudden change by applying an additional yaw moment, which is more suitable for the current working condition to the vehicle, and limits the yaw rate to a reasonable range (-23 deg/s to 18.7 deg/s) in the subsequent test. The change rate of the yaw rate before and after 1 second decreases to 42.816 deg/s^2. The analysis of vehicle trajectory indicates that the uncontrolled vehicle has excessive steering due to the rear axle side slip, which causes the vehicle to substantially deviate from the ideal trajectory, while SMC improves the vehicle motion. However, the control force is not sufficient, which causes the vehicle control effect to be inferior to the FSMC method.

As the setting of this condition is different from that of the double lane-shifting condition, the vehicle is in the extreme motion state for a long time, which causes the sideslip angle and yaw rate to be significantly greater than those of the double lane-shifting condition. Therefore, although this value is relatively large, considering the poor driving conditions, the FSMC method shows that limiting the dangerous movement of the body is more effective and ensures the normal movement posture of the body.

V. CONCLUSION

Based on the model building and AUKF centroid sideslip angle estimation, an adaptive DYC is proposed utilizing FSMC as a decision-making layer. Therefore, a DYC hierarchical control strategy that is based on vehicle state estimation is developed. For validation, two aspects of the advantages of the FSMC designed in this paper compared with traditional SMC are analyzed.

From the viewpoint of the control process, the traditional SMC is very sensitive to disturbance when it attains the sliding mode, and a small disturbance will also cause a large control variable in the traditional SMC. Thus, frequent chattering will occur in the control process, and the abrupt amplitude of change of the control variable is large, which cannot be quickly restored to normal. The FSMC designed in this paper maintains continuous discrete symbolic functions by using the fuzzy system $\hat{h}(S, \hat{\theta})$ approach and the switching term with variable gain, which avoids the problems caused by the traditional SMC.

From the point of view of the control effect, the control effect of the traditional SMC is worse than the FSMC control method designed in this paper. The reason is that the traditional SMC control method cannot be changed once the parameters are set, and the setting of parameters cannot ensure that the control effect attains the best level under each working condition. When FSMC is designed, the variable switching gain based on the fuzzy rules can adjust the

parameters in real time according to the relative position of the system, the sliding surface and its motion state. Thus, the fuzzy system $\hat{h}(S, \hat{\theta})$ always approximates the switching term of the variable gain, which guarantees the ideal control effect under any working conditions and ensures the stability and convergence of the whole system.

REFERENCES

[1] Editorial department of journal of China highway, "Review on China's automotive engineering research progress," *J. China Highway*, vol. 30, no. 6, pp. 190–197, 2017.
[2] Z. Changfu, L. Gang, and Z. Hongyu, "Study progress and outlook of chassis control technology for X-by-wire automobile," *J. China Highway*, vol. 26, no. 2, pp. 160–176, Mar. 2013.
[3] D. Xiying, L. Lin, Y. Hua, L. Xiaozhuang, and P. Yanliang, "Integrated DYC/ASR-based variable universe fuzzy control for electric vehicles," *Automobile Eng.*, vol. 36, no. 5, pp. 527–531, May 2014.
[4] L. G. H. Hai-lan, "Study on yaw moment control for electric vehicle with four-wheel in-wheel motor based on fuzzy control," in *Proc. Machinery Des. Manuf.*, Jul. 2016, pp. 26–29.
[5] W. Panpan, Y. Xiujian, and Y. Xiaoying, "Research on vehicle stability control based on optimal tire force distribution," *Agricult. Equip. Vehicle Eng.*, vol. 56, no. 2, pp. 1–6, 2018.
[6] J. Liqiang, L. Gang, and C. Pengfei, "Hierarchical control for vehicle electronic stability control system," *J. Jilin Univ.*, vol. 46, no. 6, pp. 1765–1771, 2016.
[7] W. Qidong, L. Wei, and C. Wuwei, "Sliding mode control of vehicle electronic stability program based on road identification," *Automot. Eng.*, vol. 40, no. 1, pp. 82–90, Apr. 2018.
[8] X. Lu, L. yue, and L. Bo, "Handling and stability control of distributed drive electric vehicle based on motion tracking," *J. Tongji Univ.*, vol. 45, no. 1, pp. 53–57, 2017.
[9] Z. Cong, W. Zhenchen, and C. Jv, "Sliding Mode Control of AFS+ARS+DYC for the Yaw Stability of a 4WIS-4WID Vehicle," *Automot. Eng.*, vol. 36, no. 3, pp. 304–309, Oct. 2014.
[10] L. Jinkun, *Sliding Mode Control Design and MATLAB Simulation-The Basic Theory and Design Method*, 3rd ed. Beijing, China: Tsinghua Univ. Press, 2015.
[11] A. Tota, B. Lenzo, Q. Lu, A. Sorniotti, P. Gruber, S. Fallah, and D. Smet, "On the experimental analysis of integral sliding modes for yaw rate and sideslip control of an electric vehicle with multiple motors," *Int. J. Automot. Technol.*, vol. 19, no. 5, pp. 811–823, Oct. 2018.
[12] E. Lu, W. Li, X. Yang, and Y. Liu, "Anti-disturbance speed control of low-speed high-torque PMSM based on second-order non-singular terminal sliding mode load observer," *ISA Trans.*, vol. 88, pp. 142–152, 2018.
[13] D.-H. Kim, C.-J. Kim, S.-H. Kim, C.-S. Han, and J. Y. Choi, "Development of adaptive direct yaw-moment control method for electric vehicle based on identification of yaw-rate model," in *Proc. IEEE Intell. Vehicles Symp. (IV)*, Jun. 2011, pp. 1098–1103.
[14] L. Yinong, H. Yiming, and Z. Tao, "Yaw stability control of wheel-drive electric vehicle," *J. Chongqing Univ.*, vol. 40, no. 12, pp. 24–34, 2017.
[15] J. Guo, L. Li, and K. Li, "An adaptive fuzzy-sliding lateral control strategy of automated vehicles based on vision navigation," *Vehicle Syst. Dyn.*, vol. 51, no. 10, pp. 1502–1517, 2013.
[16] J. I. Suárez, B. M. Vinagre, and Y. Q. Chen, "A fractional adaptation scheme for lateral control of an AGV," *IFAC Proc*, vol. 39, pp. 149–154, 2006.
[17] C. Chen, J. Lv, Gao, and S. Gao, and H. Liu, "Adaptive fuzzy sliding mode control algorithm based on input-output linearization for vehicle's lateral control," *IEEE Chin. Guid., Navigat. Control Conf. (CGNCC)*, Aug. 2016, pp. 1363–1368.
[18] E. Mousavinejad, Q.-L. Han, F. Yang, Y. Zhu, and L. Vlacic, "Integrated control of ground vehicles dynamics via advanced terminal sliding mode control," *Vehicle Syst. Dyn.*, vol. 55, no. 2, pp. 268–294, Oct. 2016.
[19] Y. Zhuoping, F. Yuan, and X. Lu, "Review on vehicle dynamics control of distributed drive electric vehicle," *J. Mech. Eng.*, vol. 49, no. 8, pp. 105–114, Apr. 2013.
[20] A. G. E. Esmailzadeh, "Design of a VDC system for all-wheel independent drive vehicles," *IEEE/ASME Trans. Mechatron.*, vol. 12, no. 6, pp. 632–639, Dec. 2007.
[21] Yoichi Hori. Furtur, "Future vehicle driven by electricity and Control-research on four-wheel-motored 'UOT electric march II'," *IEEE Trans. Ind. Electron.*, vol. 51, no. 5, pp. 954–962, Oct. 2004.
[22] R. Rajamani, *Vehicle Dynamics and Control*, 2nd ed. New York, NY, USA: Springer; 2012.
[23] A. Ghaffari, S. H. T. Oreh, and R. Kazemi, "An intelligent approach to the lateral forces usage in controlling the vehicle yaw rate," *Asian J. Control*, vol. 13, no. 2, pp. 213–231, Mar. 2011.
[24] Z. Tao, "Research on differential power steering and yaw torque control of electric vehicle driven by hub motor," in *Proc. College Automobile Eng.*, 2017, pp. 39–42.
[25] J. Guo, Y. Luo, and K. Li, "Adaptive fuzzy sliding mode control for coordinated longitudinal and lateral motions of multiple autonomous vehicles in a platoon," *Sci. China Technol. Sci.*, vol. 60, no. 4, pp. 576–586, Dec. 2016.
[26] J. Liqiang, W. Qingqiang, and Y. Weiqiang, "Dynamic control for four-wheel independent drive electric vehicle," *Acta Simulata Systematica Sinica*, vol. 12, pp. 3053–3055, Apr. 2005.
[27] S. Yue and Y. Fan, "Hierarchical direct yaw-moment control system design for in-wheel motor driven electric vehicle," *Int. J. Automot. Technol.*, vol. 19, no. 4, pp. 695–703, Aug. 2018.
[28] H. Chen, "Review on Vehicle Sideslip Angle Estimation," *J. Mech. Eng.*, vol. 49, no. 24, 2013.
[29] W. Chen, D. Tan, and L. Zhao, "Vehicle sideslip angle and road friction estimation using online gradient descent algorithm," *IEEE Trans. Veh. Technol.*, vol. 67, no. 12, pp. 11475–11485, Dec. 2018.
[30] L. Chen, T. Chen, X. Xu, Y. Cai, H. Jiang, and X. Sun, "Sideslip angle estimation of in-wheel motor drive electric vehicles by cascaded multi-Kalman filters and modified tire model," *Metrol. Meas. Syst.*, vol. 26, no. 1, pp. 185–208,2019.
[31] E. Joa, K. Yi, and Y. Hyun, "Estimation of the tire slip angle under various road conditions without tire–road information for vehicle stability control," *Control Eng. Pract.*, vol. 86, pp. 129–143, May 2019.
[32] M. Abe, *Vehicle Handling Dynamics-Theory and Application*, 2nd ed. Beijing, China: China Mach. Press, 2016, pp. 212–216.
[33] H. S. Kim, Y. J. Hyun, and K. H. Nam, "Disturbance observer-based sideslip angle control for improving cornering characteristics of in-wheel motor electric vehicles," *Int. J. Automot. Technol.*, vol. 19, no. 6, pp. 1071–1080, Dec. 2018.
[34] Z. Wang, Y. Qin, C. Hu, M. Dong, and F. Li, "Fuzzy observer-based prescribed performance control of vehicle roll behavior via controllable damper," *IEEE Access*, vol. 7, pp. 19471–19487, 2019.
[35] A. Norouzi, R. Kazemi, and S. Azadi, "Vehicle lateral control in the presence of uncertainty for lane change maneuver using adaptive sliding mode control with fuzzy boundary layer," in *Proc. Inst. Mech. Eng., I, J. Syst. Control Eng.*, vol. 232, no. 1, pp. 12–28, Oct. 2017.
[36] W. Cao, Y. Wu, E. Zhou, J. Li, and J. Liu, "Reliable integrated ASC and DYC control of all-wheel-independent-drive electric vehicles over CAN using a Co-design methodology," *IEEE Access*, vol. 7, pp. 6047–6059, 2019.
[37] R. Hou, L. Zhai, T. Sun, Y. Hou, and G. Hu, "Steering stability control of a four in-wheel motor drive electric vehicle on a road with varying adhesion coefficient," *IEEE Access*, vol. 7, pp. 32617–32627, 2019.

HOUZHONG ZHANG was born in Tai'an, Jiangxi, China, in 1978. He received the Ph.D. degree in vehicle engineering from Tongji University, Shanghai, China, in 2012. He was a Software Engineer with Shanghai Electric Drive Company Ltd., from 2009 to 2010, responsible for the control and testing of automotive motors. He is currently a Master's Supervisor with the Automotive Engineering Research Institute, Jiangsu University.

His research interests include distributed drive electric vehicle, simulation, and control of vehicle dynamic performance.

JIASHENG LIANG was born in Shijiazhuang, Hebei, China, in 1996. He received the bachelor's degree from the Engineering College, Anhui Agricultural University, Hefei, Anhui, China, in 2018. He is currently pursuing the master's degree with the Automotive Engineering Research Institute, Jiangsu University.

His current research interests include active safety of automobile and state estimation of automobile.

HAOBIN JIANG was born in Qidong, Jiangsu, China, in 1969. He received the B.S. degree in agricultural mechanization from Nanjing Agricultural University, Nanjing, China, in 1991, and the M.S. and Ph.D. degrees in vehicle engineering from Jiangsu University, Zhenjiang, China, in 1994 and 2000, respectively.

His research interests include vehicle dynamic performance analysis and electrical control technology.

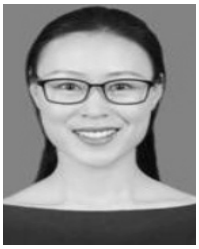

YINGFENG CAI was born in Nantong, Jiangsu, China, in 1985. She received the B.S., M.S., and Ph.D. degrees from the School of Instrument Science and Engineering, Southeast University, Nanjing, China. In 2013, she joined the Automotive Engineering Research Institute, Jiangsu University, as an Assistant Professor.

Her research interests include computer vision, intelligent transportation systems, and intelligent automobiles.

XING XU was born in Haian, Jiangsu, China, in 1979. He received the B.S. degree in vehicle engineering, the M.S. degree in control theory and control engineering, and the Ph.D. degree in agricultural electrification and automation from Jiangsu University, Zhenjiang, China, in 2002, 2006, and 2010, respectively.

He is currently a Professor and a Doctoral Supervisor with the Automotive Engineering Research Institute, Jiangsu University. His research interests include the modeling, identification, optimization, fault diagnosis, and control of vehicle dynamic systems.